RSC Advances

PAPER

View Article Online
View Journal | View Issue

Cite this: *RSC Adv.*, 2025, **15**, 50419

Deciphering the donor–acceptor order: impact of acceptor positioning on the optical properties of anthraquinone-carbazole-cyanostilbenes

A. Afrin and Chinna Ayya Swamy P. *

We report a systematic investigation of anthraquinone–carbazole–cyanostilbene conjugates arranged in two distinct connectivity patterns: **AQCZCS** and **CZCSAQ**. Despite having identical donor and acceptor units, subtle differences in donor–acceptor ordering profoundly impact their optical and excited-state properties. Both isomers exhibit broad, structureless emission characteristic of charge-transfer (CT) states, with maxima at 635 nm (**AQCZCS**) and 700 nm (**CZCSAQ**), corresponding to a pronounced bathochromic shift ($\Delta\lambda$ ~65 nm). Solution-phase emission reflects connectivity-dependent shifts, confirming strong donor–acceptor communication. In the solid state, **AQCZCS** emits vivid orangish red (610 nm) that shifts to deep red (645 nm) upon mechanical stimulation, while **CZCSAQ** shows red emission that further bathochromically responds under force, highlighting the tunable mechanochromic behavior. Quantum yields of 2.7% (**AQCZCS**) and 1.8% (**CZCSAQ**) demonstrate the effect of topology on emissive efficiency. These findings establish robust structure–property correlations and provide design principles for multifunctional solid-state emitters with highly tunable CT-driven emission across the visible spectrum.

Received 16th October 2025
Accepted 10th December 2025

DOI: 10.1039/d5ra07931d

rsc.li/rsc-advances

Introduction

Organic π-conjugated luminophores are central to modern optoelectronics, finding widespread use in organic light-emitting diodes (OLEDs),[1–6] sensing platforms,[7–10] and bioimaging.[11–15] The continuous drive toward next-generation materials have inspired strategies to overcome classical limitations such as aggregation-caused quenching (ACQ), while also enabling advanced photophysical phenomena like aggregation-induced emission (AIE),[16,17] solvatochromism,[18–20] mechanochromism,[21–25] and thermally activated delayed fluorescence (TADF).[26–30] Central to these efforts is the donor–acceptor (D–A) design principle, where the careful interplay between electron-rich and electron-deficient fragments allows tuning of emission color, charge-transfer character, and excited-state dynamics.[31–35] Among the wide variety of building blocks, carbazole has emerged as an important electron donor due to its strong donating ability, rigid framework, and good photostability.[36–40] Cyanostilbene is a versatile π-acceptor/spacer, well known for its twisted structure that suppresses ACQ and promotes AIE.[41–44] On the other hand, anthraquinone (AQ) is a classic diketone acceptor with strong electron-withdrawing carbonyl groups and a rigid fused backbone that efficiently lowers the LUMO and enhances spin–orbit coupling.[45–50] The combination of these units provides a robust molecular platform to engineer solid-state emitters with finely tunable optical properties.

Over the years, we have systematically explored carbazole-based scaffolds to understand how structure governs solid-state emission. Early studies on carbazole–anthracene conjugates showed that subtle changes in acceptor unit substitutions can affect emission, quantum yield, and aggregation.[51] Extending this to carbazole–cyanostilbene systems with varied π-spacers revealed that conjugation length effectively tunes charge transfer, AIE and MFC behavior.[52,53] Recently, we have focused on how positional changes of the benzothiazole acceptor influence emission color, molecular packing, and mechanochromic behavior.[54] While donor–acceptor chemistry has been widely explored, the role of positional isomerism *i.e.*, the order in which donor and acceptor units are connected within the conjugated backbone remains comparatively underexplored. Even when the same fragments are present, their sequence can dictate the extent of orbital overlap, conjugation, and intermolecular packing, leading to pronounced differences in photophysical behavior. Positional variations can modulate emission wavelengths, solvatochromic shifts, AIE activity, and even the singlet-triplet energy gap (ΔE_{ST}), offering a subtle yet powerful lever for materials design. In this work, we focus on anthraquinone–carbazole–cyanostilbene conjugates, where the same donor (carbazole), cyanostilbene, and acceptor (anthraquinone) units are arranged in two distinct connectivity patterns (**AQCZCS** and **CZCSAQ**) (Chart 1). By systematically comparing these positional isomers, we uncover how subtle

Main Group Organometallics Optoelectronic Materials and Catalysis Lab, Department of Chemistry, National Institute of Technology, Calicut, 673601, India. E-mail: swamy@nitc.ac.in

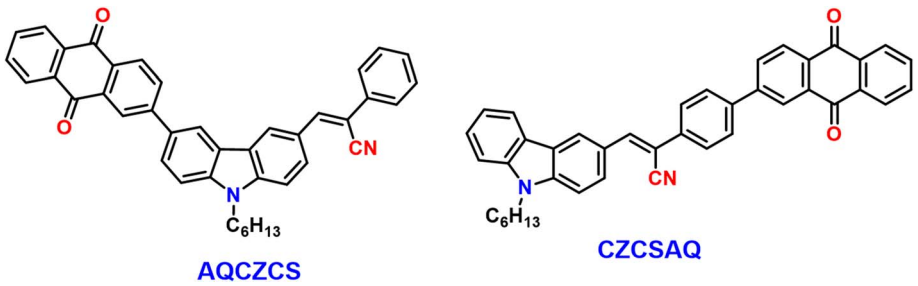

Chart 1 Molecular structures of the isomers.

differences in donor–acceptor ordering governs their optical and excited-state properties. Through experimental photophysics, AIE and solvatochromism studies, and theoretical calculations, we establish clear structure–property correlations that highlight the critical role of connectivity in dictating emission behavior. These findings not only deepen the understanding of positional effects in organic luminophores but also provide guiding principles for the rational design of multifunctional solid-state emitters.

Results and discussions

Synthesis and characterisation

The synthetic route toward the anthraquinone–carbazole–cyanostilbene conjugates (**AQCZCS** and **CZCSAQ**) is drawn in Scheme 1. Both positional isomers were constructed *via* a stepwise strategy including Suzuki–Miyaura cross-coupling and Knoevenagel condensation. For **AQCZCS**, 2-bromoanthracene-9,10-dione was first coupled with 9-hexyl-6-(4,4,5,5-tetramethyl-1,3,2-dioxaborolan-2-yl)-9H-carbazole-3-carbaldehyde using Suzuki–Miyaura reaction conditions to afford the corresponding aldehyde intermediate. Subsequent Knoevenagel condensation with benzylacetonitrile furnished the desired conjugate in moderate yield. In contrast, the **CZCSAQ** isomer was obtained by first synthesizing the carbazole-cyanostilbene intermediate. This was achieved by condensing 9-hexyl-9H-carbazole-3-carbaldehyde with 4-bromobenzylacetonitrile to yield a carbazole-cyanostilbene derivative, which was then subjected to Suzuki–Miyaura borylation. In this pathway, the key boronic ester (Z)-3-(9-hexyl-9H-carbazol-3-yl)-2-(4-(4,4,5,5-tetramethyl-1,3,2-dioxaborolan-2-yl)phenyl)acrylonitrile, undergoes Suzuki cross coupling reaction with 2-bromoanthracene-9,10-dione to yield **CZCSAQ**. The chemical structures of **AQCZCS** and **CZCSAQ** were confirmed by ^{1}H and ^{13}C NMR spectroscopy together with high-resolution mass spectrometry (HRMS). The ^{1}H NMR spectra of both isomers displayed sharp, well-resolved resonances corresponding to the product. The integration values were fully consistent with the proposed structures, while the characteristic downfield-shifted protons of the anthraquinone moiety and the vinylic proton signals of the cyanostilbene unit provided clear analytic evidence of successful conjugation. The ^{13}C NMR spectra likewise exhibited well-defined signals for all aromatic and aliphatic carbons, including the carbonyl carbons of the anthraquinone group and the cyano carbon of the cyanostilbene. Importantly, no solubility issues were encountered, allowing the complete assignment of all major carbon resonances. Further support came from ESI-HRMS analysis, which revealed molecular ion peaks ($[M]^+$ or $[M + H]^+$) in agreement with the calculated exact masses, thereby confirming the molecular formulations of both positional isomers. Taken together, the combined NMR and HRMS data firmly establish the successful synthesis of **AQCZCS** and **CZCSAQ**.

Photophysical properties in solution

The absorption and emission spectra of **AQCZCS** and **CZCSAQ** were first recorded in THF (Con. $= 1.0 \times 10^{-5}$ M) (Fig. 1). Both compounds display intense absorptions in the 240–300 nm region arising predominantly from localized π–π* transitions of the aromatic units, while the additional bands extending into the 300–350 nm region can be attributed *n*–π* transitions commonly observed in anthraquinone-based chromophores.[55] A weaker, broadened band extending into the visible region (370–430 nm) is evident, which can be assigned to charge-transfer (CT) interactions involving the anthraquinone acceptor. Interestingly, **CZCSAQ** exhibits a more red-shifted and broader absorption profile compared to **AQCZCS**, reflecting stronger donor–acceptor coupling when the anthraquinone unit is positioned at the terminal end of the π-conjugated pathway. Upon excitation at the ICT band, both **AQCZCS** and **CZCSAQ** exhibited broad, structureless emission profiles characteristic of charge-transfer (CT) states, with maxima at 635 nm and 700 nm, respectively. The positional variation of the anthraquinone fragment induced a pronounced bathochromic shift of $\Delta\lambda \sim 65$ nm, underscoring the sensitivity of excited-state energies to donor–acceptor topology. Notably, the emission profile of **CZCSAQ** is broader and extends further into the near-infrared region, indicative of enhanced charge delocalization and stronger electronic communication across the conjugated backbone. These findings establish that although both isomers are constructed from identical donor–acceptor components, the specific placement of anthraquinone critically governs their electronic structures, resulting in distinct optical bandgaps and emission colors. Absolute quantum yields (ϕ_f) in THF were relatively low, $\phi = 7\%$ (**AQCZCS**) and 1.8% (**CZCSAQ**), consistent with the strong electron-accepting nature of anthraquinone and the prevalence of nonradiative deactivation pathways.

Solvatochromism

The UV-vis absorption spectra of both **AQCZCS** and **CZCSAQ** remained invariant across solvents of varying polarity, with the lowest-energy absorption band (ICT) consistently centered at

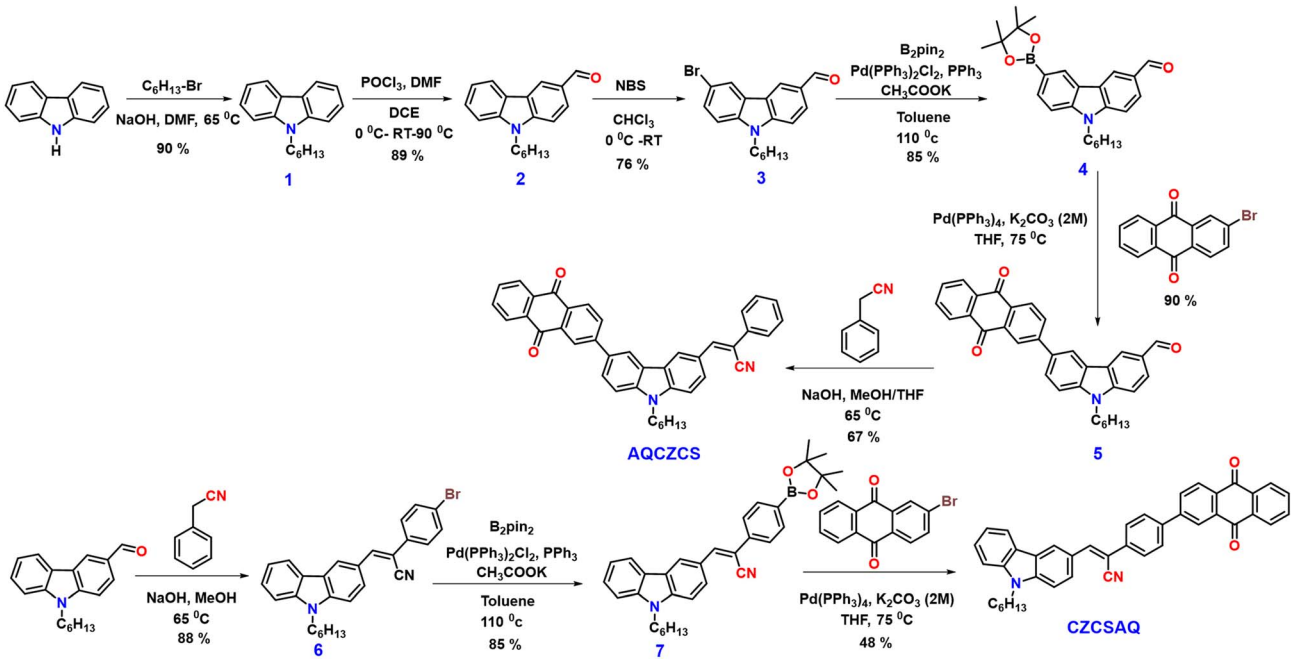

Scheme 1 Synthetic scheme for the target isomers.

the same wavelength (Fig. S15). This insensitivity of the ground-state absorption to solvent environment suggests that the lowest-energy transitions possess predominantly locally excited (LE) character, with minimal redistribution of charge in the ground state. In contrast, the emission spectra revealed strong positive solvatochromism, characteristic of excited states with pronounced charge-transfer (CT) character. For **AQCZCS**, the emission maximum shifted from 550 nm in toluene to 635 nm in THF, while **CZCSAQ** showed an even more dramatic shift from 530 nm to >700 nm across the same solvent range. The greater solvatochromic response of **CZCSAQ** indicates that positioning the anthraquinone at the opposite end of the π-conjugated framework enhances donor–acceptor electronic communication, leading to stronger stabilization of the CT excited state in polar environments. The photoluminescence quantum yields (PLQYs) of both compounds were measured in various solvents to correlate emission efficiency with solvent polarity (Table S1). **AQCZCS** exhibited a high PLQY of 56.1% in toluene, which decreased significantly to 7% in THF, while **CZCSAQ** showed comparatively lower efficiencies of 5.0% and 1.8%, respectively. The pronounced drop in PLQY with increasing polarity further confirms the solvent-dependent

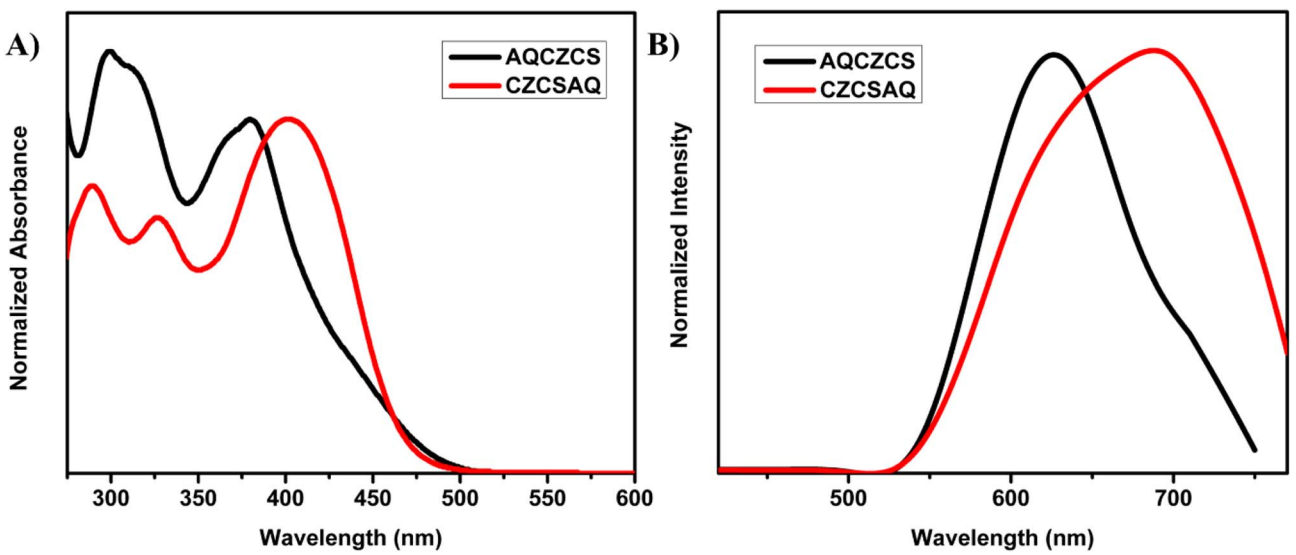

Fig. 1 (A) Normalized absorption and (B) normalized emission spectra of isomers **AQCZCS** and **CZCSAQ** in THF (Con. 10 μM, λ_{ex} = 380 nm for **AQCZCS** and λ_{ex} = 400 nm for **CZCSAQ**).

charge-transfer nature of the emissive states. These findings reinforce the notion that while the ground states of the two isomers are relatively unaffected by solvent polarity, their excited states are highly sensitive to both molecular topology and solvent polarity effects.

Aggregation-induced emission (AIE) studies

The aggregation-induced emission (AIE) properties of **AQCZCS** and **CZCSAQ** were examined in DMSO/H_2O mixtures with varying water fractions (f_w), where the addition of water gradually reduces solubility and induces molecular aggregation (Fig. 2). For **AQCZCS**, the emission intensity showed no change at low water fractions but began to rise noticeably at $f_w = 30\%$, reaching a maximum at $f_w = 40\%$, after which a steady decrease was observed at higher water fractions. In contrast, **CZCSAQ** exhibited an aggregation-induced emission response, with the luminescence peaking at $f_w = 60\%$ and again showing a decline at higher water fractions. Notably, at $f_w = 90\%$, **CZCSAQ** displayed a secondary enhancement in emission intensity with a red-shifted emission maximum, suggesting the formation of more compact and emissive aggregates at very high-water

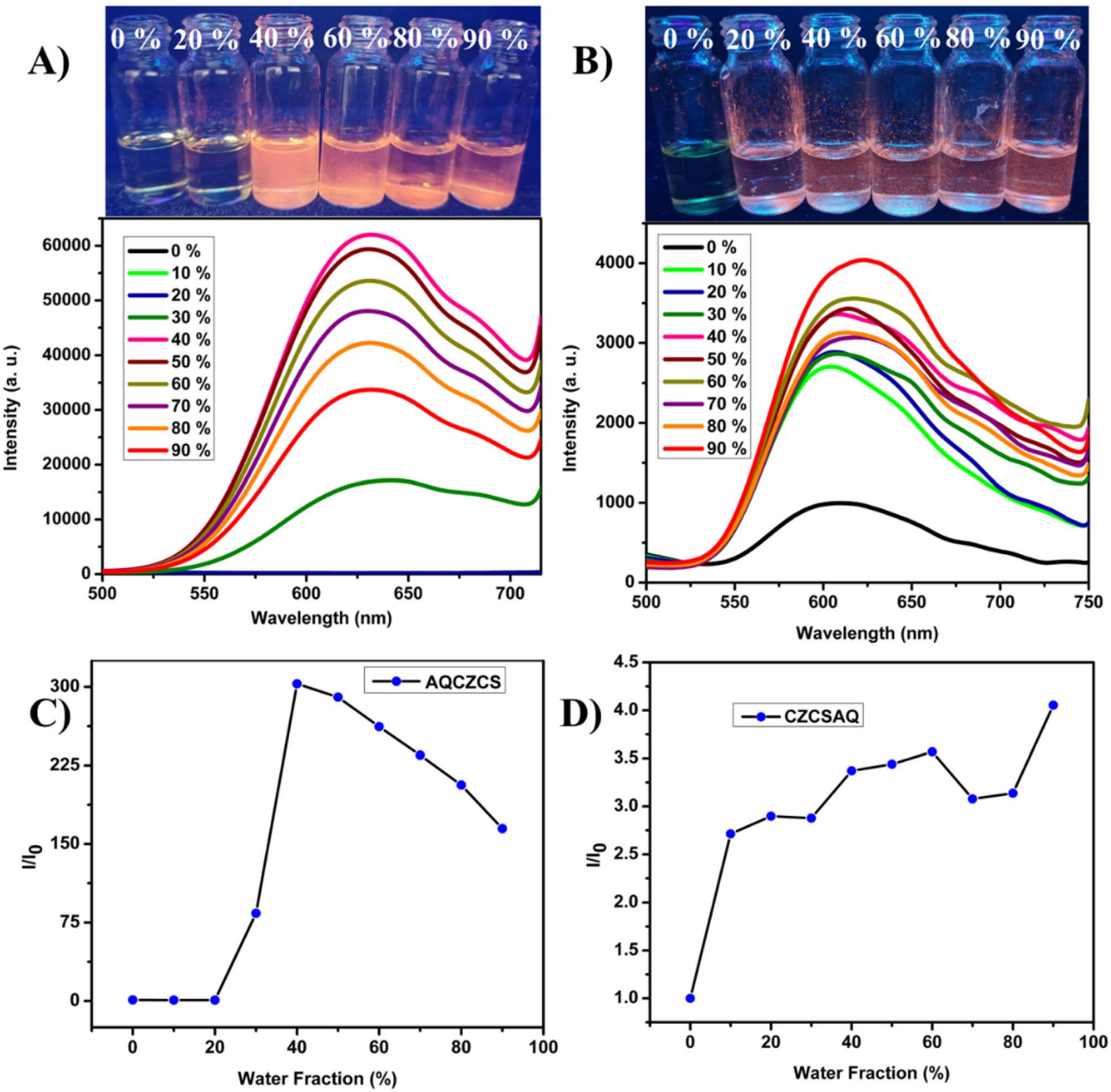

Fig. 2 Fluorescence spectra of (A) **AQCZCS** and (B) **CZCSAQ** in DMSO-water mixtures with different water fractions. Digital photos taken for the various water fractions under UV 365 nm lamp are displayed at the top of the spectra. I/I_0 plots of (C) **AQCZCS** and (D) **CZCSAQ** with different fractions of water (Con. 10 μM, $\lambda_{ex} = 380$ nm for **AQCZCS** and $\lambda_{ex} = 400$ nm for **CZCSAQ**). (Instrumental parameters: excitation slit width and emission slit width = 20 nm).

content. Importantly, the maximum emission intensity of **AQCZCS** was nearly fifteen times higher than that of **CZCSAQ**, underscoring the much greater efficiency of aggregate-induced restriction of intramolecular motions in the former. The different aggregation behaviors of the two isomers highlight the role of anthraquinone positioning in dictating molecular packing preferences and aggregation pathways. The emission maxima closely correlated with morphological observations from scanning electron microscopy (SEM) and particle size distributions obtained by dynamic light scattering (DLS) (Fig. S17 and S18). In both cases, the strongest emission coincided with the largest aggregate sizes, indicating that the restriction of intramolecular motions (RIM) in densely packed aggregates is the primary contributor to the observed AIE activity.[56] These results underscore that while both positional isomers display aggregation-enhanced emission, the distinct water-fraction dependence and large disparity in emission efficiencies reflect different aggregation modes governed by donor–acceptor topology.

Solid state emission and mechanochromism

In the solid state, both isomers displayed distinct photophysical characteristics influenced by the position of the anthraquinone unit. **AQCZCS** exhibited vivid-orangish red emission centered at 610 nm with a quantum yield of 2.7%, while **CZCSAQ** showed a further red-shifted emission at 620 nm with a quantum yield of 1.8% (Fig. 3). The red-shifted profile of **CZCSAQ** pushes its emission closer to the deep-red region, underscoring how anthraquinone positioning governs the extension of conjugation and stabilization of the excited state. Upon mechanical grinding, both isomers reveal mechanochromic fluorescence responses. **AQCZCS** undergoes a remarkable red-shift from 610 to 645 nm, whereas **CZCSAQ** shifts from 620 to 635 nm. PXRD analysis confirms that these optical transitions originate from a crystalline-to-amorphous phase transformation, where disrupted molecular packing enhances intermolecular interactions (Fig. S19).[57] Notably, the mechanochromic response is irreversible in both systems. Taken together, these results show that the donor–acceptor sequence not only dictates emission color: from orange to near deep-red, but also modulates mechanochromic sensitivity. The larger shift of **AQCZCS** contrasts with the intrinsically redder emission of **CZCSAQ**, underscoring a trade-off between mechanochromic amplitude and spectral positioning. Such insights provide valuable guidelines for designing responsive solid-state luminophores.

Theoretical studies

Quantum-chemical calculations were undertaken to provide a molecular-level understanding of the structure–property relationships in **AQCZCS** and **CZCSAQ**. Ground-state geometries were optimized using DFT (B3LYP/6-31G(d,p)), and the absence of imaginary frequencies confirmed that both molecules are true minima.[58] Frontier molecular orbital (FMO) analysis revealed a pronounced donor–acceptor separation. The HOMO density is largely distributed over the carbazole and cyanostilbene segments, reflecting their strong electron-donating and conjugated nature, whereas the LUMO is entirely localized on the anthraquinone core. This orbital distribution highlights the charge-transfer (CT) character of the lowest-energy transitions. Interestingly, the HOMO–LUMO energy gap was calculated to be 2.63 eV for **AQCZCS** and slightly narrower at 2.54 eV for **CZCSAQ**, in line with the experimentally observed red-shifted emission of the latter. Excited-state properties were further examined by TD-DFT, using both B3LYP and M06 functionals in the presence of solvent (PCM, THF). While both functionals reproduced the main CT absorption band, M06 delivered excitation energies and oscillator strengths in closest agreement with experiment. Natural transition orbital (NTO) analysis further confirmed the intramolecular charge transfer nature of the S_1 state, with both isomers displaying clear spatial separation between the hole and particle densities localized on the donor and acceptor segments, respectively (Fig. 4).

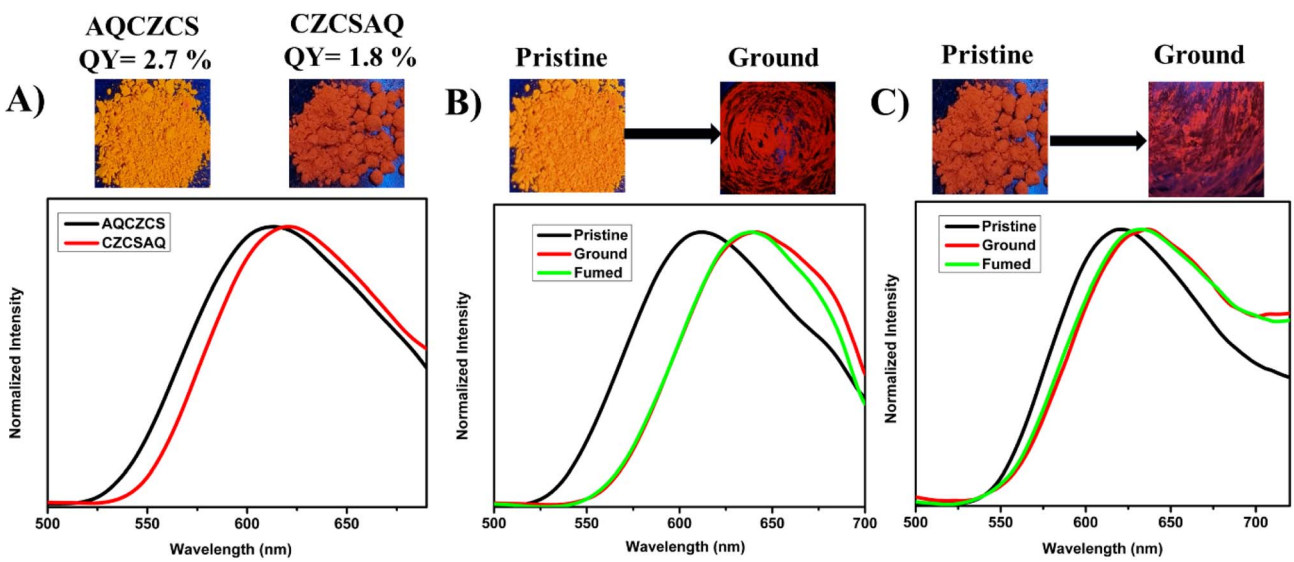

Fig. 3 (A) Solid-state emission spectra of isomers, MFC responses of (B) **AQCZCS** and (C) **CZCSAQ**.

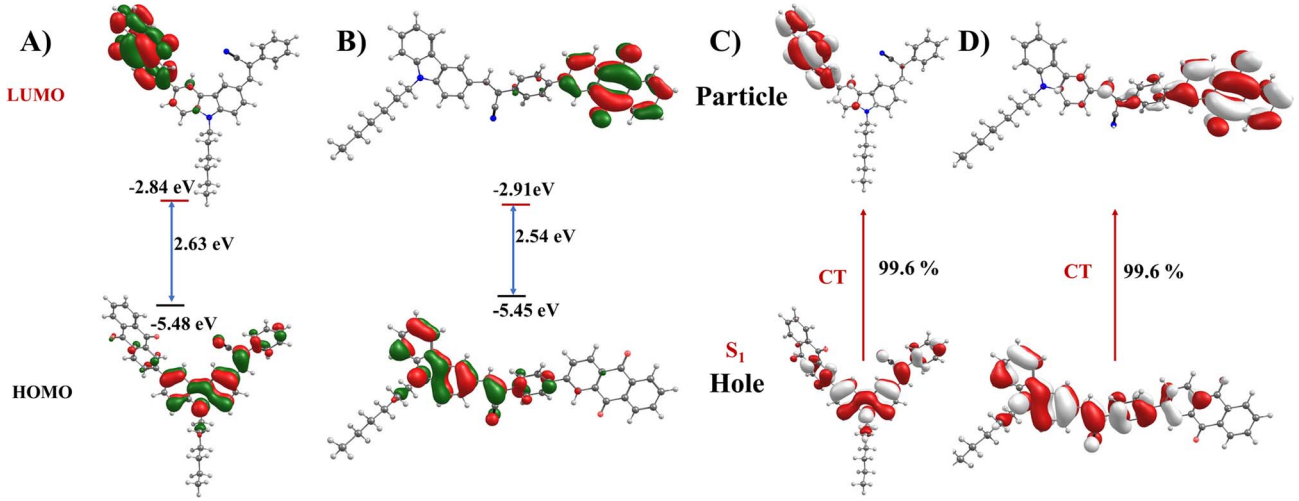

Fig. 4 FMO analysis and calculated energy gaps of isomers (A) **AQCZCS** and (B) **CZCSAQ**. Natural transition orbitals (NTOs) calculated for S_1 of (C) **AQCZCS** and (D) **CZCSAQ** using M06 functional and 6-31G(d, p) basis set.

Thermal properties

The thermal stability of **AQCZCS** and **CZCSAQ** was evaluated by thermogravimetric analysis (TGA) and differential scanning calorimetry (DSC). As shown in Fig. S22(A), both compounds exhibited good stability with decomposition temperatures (T_d, defined at 5% weight loss) well above 380 °C. Specifically, **AQCZCS** retained its structural integrity up to ~410 °C, while **CZCSAQ** showed an onset of decomposition at ~380 °C. Such high decomposition temperatures underscore the determined nature of the carbazole–cyanostilbene–anthraquinone framework, which is advantageous for practical applications in optoelectronic devices that require long-term thermal endurance. The DSC thermograms (Fig. S22(B)) further revealed distinct thermal transitions. **AQCZCS** displayed a relatively broad endothermic feature around 150 °C, likely corresponding to a phase transition. In contrast, CZCSAQ showed a sharp and well-defined endothermic peak at ~210 °C, corresponding to its melting point, followed by a secondary thermal event near ~230 °C that is attributed to the onset of thermal degradation.[59] During the cooling cycle, **CZCSAQ** also displayed prominent exothermic crystallization peaks, indicating strong recrystallization tendencies. The presence of multiple endothermic and exothermic features for **CZCSAQ** highlights its greater propensity for phase reorganization compared to **AQCZCS**. Inclusive, the thermal analyses confirm that both isomers are thermally robust, with decomposition temperatures well beyond those typically required for device fabrication.

Conclusions

This study demonstrates that the positional arrangement of anthraquinone within carbazole–cyanostilbene conjugates exerts a decisive influence on their photophysical behavior. **AQCZCS** and **CZCSAQ**, despite having identical donor, and acceptor units, display different emission profiles: in the solid state, **AQCZCS** shifts from vivid orangish red to deep red upon mechanical stimulation, whereas **CZCSAQ** exhibits red emission with slight bathochromic shift. These shifts highlight the tunability of solid-state emission through subtle positional connectivity of the acceptor unit. Solution-phase emission mirrors these connectivity effects, confirming strong donor–acceptor electronic communication. The pronounced bathochromic shifts, broad CT-character emission, and topology-dependent quantum yields underscore the critical role of donor–acceptor ordering in dictating excited-state properties. Altogether, these findings provide a clear structure–property blueprint for designing multifunctional solid-state luminophores with tunable orange-to-deep-red emission and responsive mechanochromic behavior.

Conflicts of interest

The authors declare no competing financial interest.

Data availability

The data underlying this study are available in the published article and its supporting information (SI). Supplementary information: ^{1}H NMR, ^{13}C NMR, HRMS, and characterization data for the isomers, photophysical data, PXRD, SEM, DLS, DFT and TD-DFT results (PDF). See DOI: https://doi.org/10.1039/d5ra07931d.

Acknowledgements

CAS P thanks, SERB/EEQ/2021/000180 for funding and support. A. A thanks the National Institute of Technology, Calicut, for GATE-SRF fellowship. The authors acknowledge the Centre for Materials Characterisation NIT Calicut for NMR, PXRD facilities, HRMS (DST-FIST) and Centre for Computational Modelling and Simulations NIT Calicut. We would like to thank the SEM Centre, the Department of Materials Science and

Engineering, National Institute of Technology Calicut for the SEM facility.

References

1 S. J. Zou, Y. Shen, F. M. Xie, J. D. Chen, Y. Q. Li and J. X. Tang, Recent advances in organic light-emitting diodes: toward smart lighting and displays, *Mater. Chem. Front.*, 2020, **4**, 788.

2 A. Salehi, X. Fu, D. H. Shin and F. So, Recent advances in OLED optical design, *Adv. Funct. Mater.*, 2019, **29**, 1808803.

3 X. Wu, S. Ni, C. H. Wang, W. Zhu and P. T. Chou, Comprehensive Review on the Structural Diversity and Versatility of Multi-Resonance Fluorescence Emitters: Advance, Challenges, and Prospects toward OLEDs, *Chem. Rev.*, 2025, **125**, 6685–6752.

4 M. K. Bera, P. Pal and S. Malik, Solid-state emissive organic chromophores: design, strategy and building blocks, *J. Mater. Chem. C*, 2020, **8**, 788–802.

5 S. Banerjee, P. Singh, P. Purkayastha and S. Kumar Ghosh, Evolution of Organic Light Emitting Diode (OLED) Materials and their Impact on Display Technology, *Chem.–Asian J.*, 2025, **20**, e202401291.

6 M. Gao and B. Z. Tang, Fluorescent sensors based on aggregation-induced emission: recent advances and perspectives, *ACS Sens.*, 2017, **2**, 1382.

7 L. Basabe-Desmonts, D. N. Reinhoudt and M. CregoCalama, Design of fluorescent materials for chemical sensing, *Chem. Soc. Rev.*, 2007, **36**, 993–1017.

8 L. Chen, P. Y. Fu, H. P. Wang and M. Pan, Excited-state intramolecular proton transfer (ESIPT) for optical sensing in solid state, *Adv. Opt. Mater.*, 2021, **9**, 2001952.

9 Z. Zhao, H. Zhang, J. W. Lam and B. Z. Tang, Aggregation-induced emission: new vistas at the aggregate level, *Angew. Chem., Int. Ed.*, 2020, **59**, 9888–9907.

10 S. Jaiswal, S. Das, S. Kundu, I. Rawal, P. Anand and A. Patra, Progress and perspectives: fluorescent to long-lived emissive multifunctional probes for intracellular sensing and imaging, *J. Mater. Chem. C*, 2022, **10**, 6141.

11 K. Li, T. B. Ren, S. Huan, L. Yuan and X. B. Zhang, Progress and perspective of solid-state organic fluorophores for biomedical applications, *J. Am. Chem. Soc.*, 2021, **143**, 21143–21160.

12 Y. Chen, Recent advances in AIEgens for three-photon fluorescence bioimaging, *Mater. Today Chem.*, 2022, **25**, 00975.

13 Y. Chen, S. Wang and F. Zhang, Near-infrared luminescence high-contrast *in vivo* biomedical imaging, *Nat. Rev. Bioeng.*, 2023, **1**, 60–78.

14 H. Cao, Y. Gao, B. Wu, J. Zhang, L. Wang, P. Wei, L. Liu, H. Zou, H. Zhou, Z. Zheng and B. Z. Tang, Tuning Molecular Packing by Twisting Structure to Facilely Construct Highly Efficient Solid-State Fluorophores for Two-Photon Bioimaging and Photodynamic Therapy, *Adv. Funct. Mater.*, 2024, **34**, 2315692.

15 (*a*) D. Barman, K. Narang, R. Parui, N. Zehra, M. N. Khatun, L. R. Adil and P. K. Iyer, Review on recent trends and prospects in π-conjugated luminescent aggregates for biomedical applications, *Aggregate*, 2022, **3**, e172; (*b*) Y. Hu, X. Gao, J. Ma, Z. Shangguan, L. Chen, G. Zhang, X. S. Zhang, C. Li, Y. Li and D. Zhang, New AIE Emitters from the Unexpected Boron Tribromide/Boron Trichloride-mediated Cyclization Reaction and Application for Fluorescence Imaging of Lipid Droplets, *Aggregate*, 2025, **6**, e735.

16 J. Luo, Z. Xie, J. W. Lam, L. Cheng, H. Chen, C. Qiu, H. S. Kwok, X. Zhan, Y. Liu, D. Zhu and B. Z. Tang, Aggregation-induced emission of 1-methyl-1, 2, 3, 4, 5-pentaphenylsilole, *Chem. Commun.*, 2001, 1740.

17 J. Mei, N. L. C. Leung, R. T. K. Kwok, J. W. Y. Lam and B. Z. Tang, Aggregation-Induced Emission: Together We Shine, United We Soar, *Chem. Rev.*, 2015, **115**, 11718–11940.

18 A. Liu, Q. Zhang, L. Pan, F. Yang, D. Lin and C. Jiang, Donor–Acceptor Type Solvatochromic Flavonoid Materials Fluorphores for Polarity Sensing and Real-Time Temperature Monitoring, *Adv. Funct. Mater.*, 2025, **35**, 2415250.

19 H. Liu, H. Zhu, B. Liu, J. Bai, J. Peng, H. Zhang and J. Jia, AIE-active DAD (D′) dicyanodiaryl ethylene derivatives: solvatochromism, aggregation-induced emission and high-contrast mechanofluorochromism, *J. Lumin.*, 2025, **279**, 121034.

20 J. Zhou, Y. Jiang, Q. Jiang, S. Lin, Z. Chen, M. Ji, X. Gou, L. Peng and Y. Fang, Improved Solvatochromism and Quantum Yields in Acridine through Polarity-Enhanced π-Conjugation, *J. Phys. Chem. Lett.*, 2025, **16**, 4853–4860.

21 Y. Sun, Z. Lei and H. Ma, Twisted aggregation-induced emission luminogens (AIEgens) contribute to mechanochromism materials: a review, *J. Mater. Chem. C*, 2022, **10**, 14834–14867.

22 Z. Chi, X. Zhang, B. Xu, X. Zhou, C. Ma, Y. Zhang, S. Liu and J. Xu, Recent advances in organic mechanofluorochromic materials, *Chem. Soc. Rev.*, 2012, **41**, 3878–3896.

23 R. Misra, R. Gavale and F. Khan, Polymorphism in mechanochromic luminogens: recent advances and perspectives, *J. Mater. Chem. C*, 2025, **13**, 1063–1129.

24 Y. Hu, C. Qi, D. Ma, D. Yang and S. Huang, Multicolor recordable and erasable photonic crystals based on on-off thermoswitchable mechanochromism toward inkless rewritable paper, *Nat. Commun.*, 2024, **15**, 5643.

25 P. Shi, Y. Duan, W. Wei, Z. Xu, Z. Li and T. Han, A turn-on type mechanochromic fluorescent material based on defect-induced emission: implication for pressure sensing and mechanical printing, *J. Mater. Chem. C*, 2018, **6**, 2476–2482.

26 T. Zhang, Y. Xiao, H. Wang, S. Kong, R. Huang, V. Ka-Man Au, T. Yu and W. Huang, Highly twisted thermally activated delayed fluorescence (TADF) molecules and their applications in organic light-emitting diodes (OLEDs), *Angew. Chem., Int. Ed.*, 2023, **62**, e202301896.

27 Y. Liu, C. Li, Z. Ren, S. Yan and M. R. Bryce, All-organic thermally activated delayed fluorescence materials for organic light-emitting diodes, *Nat. Rev. Mater.*, 2018, **3**, 1.

28 T. Huang, W. Jiang and L. Duan, Recent progress in solution processable TADF materials for organic light-emitting diodes, *J. Mater. Chem. C*, 2018, **6**, 577.

29 H. Wang, Y. Yuan, Z. Wang and Y. Wang, Boosting organic light-emitting diodes technology using thermally activated delayed fluorescent emitters: a review, *ACS Appl. Eng. Mater.*, 2024, **2**, 781–810.

30 M. A. Bryden and E. Zysman-Colman, Organic thermally activated delayed fluorescence (TADF) compounds used in photocatalysis, *Chem. Soc. Rev.*, 2021, **50**, 7587–7680.

31 (*a*) X. Chen, X. Zhang, X. Xiao, Z. Wang and J. Zhao, Recent Developments on Understanding Charge Transfer in Molecular Electron Donor-Acceptor Systems, *Angew. Chem., Int. Ed.*, 2023, **62**, e202216010; (*b*) M. Liang, L. Liu, Y. Sun, J. Li, L. E. Zhang, X. Jiang and W. Wu, Furan-modified thiadiazolo quinoxaline as an electron acceptor for constructing second near-infrared aggregation-induced emission fluorophores for beyond 1300 nm fluorescence/photoacoustic imaging and photothermal therapy, *Aggregate*, 2024, **5**, e458.

32 Z. Chen, H. Qin, Y. Yin, D. D. Deng, S. Y. Qin, N. Li, K. Wang and Y. Sun, Full-color emissive D-D-A carbazole luminophores: red-to-NIR mechano-fluorochromism, aggregation-induced near-infrared emission, and application in photodynamic therapy, *Chem. – Eur. J.*, 2023, **29**, e202203797.

33 T. Song, H. Liu, J. Ren and Z. Wang, Achieving TADF and RTP with Stimulus-Responsiveness and Tunability from Phenothiazine-Based Donor– Acceptor Molecules, *Adv. Opt. Mater.*, 2024, **12**, 2301215.

34 X. Zhang, X. Liu, M. Taddei, L. Bussotti, I. Kurganskii, M. Li, X. Jiang, L. Xing, S. Ji, Y. Huo and J. Zhao, Red Light-Emitting Thermally-Activated Delayed Fluorescence of Naphthalimide-Phenoxazine Electron Donor-Acceptor Dyad: Time-Resolved Optical and Magnetic Spectroscopic Studies, *Chem. – Eur. J.*, 2022, **28**, e202200510.

35 A. Afrin and P. C. A. Swamy, Symphony of light: AIE and MFC in carbazole-based cyanostilbenes, *J. Mater. Chem. C*, 2024, **12**, 1923–1944.

36 J. Yin, Y. Ma, G. Li, M. Peng and W. Lin, A versatile small-molecule fluorescence scaffold: Carbazole derivatives for bioimaging, *Coord. Chem. Rev.*, 2020, **412**, 213257.

37 S. Oner and M. R. Bryce, A review of fused-ring carbazole derivatives as emitter and/or host materials in organic light emitting diode (OLED) applications, *Mater. Chem. Front.*, 2023, **7**, 4304.

38 R. K. Konidena, K. J. Thomas and J. W. Park, Recent advances in the design of multi-substituted carbazoles for optoelectronics: synthesis and structure-property outlook, *ChemPhotoChem*, 2022, **6**, 202200059.

39 B. Wex and B. R. Kaafarani, Perspective on carbazole-based organic compounds as emitters and hosts in TADF applications, *J. Mater. Chem. C*, 2017, **5**, 8622.

40 P. Mahalingavelar and S. Kanvah, α-Cyanostilbene: a multifunctional spectral engineering motif, *Phys. Chem. Chem. Phys.*, 2022, **24**, 23049–23075.

41 C. Hang, H. W. Wu and L. L. Zhu, π-Conjugated cyanostilbene-based optoelectric functional materials, *Chin. Chem. Lett.*, 2016, **27**, 1155–1165.

42 B. K. An, J. Gierschner and S. Y. Park, π-Conjugated cyanostilbene derivatives: a unique self-assembly motif for molecular nanostructures with enhanced emission and transport, *Acc. Chem. Res.*, 2012, **45**, 544–554.

43 W. Qu, X. Niu, H. Ma, Y. Liu, Z. Feng and S. Zhu, High contrast stimuli-responsive fluorescence emitters based on carbazole-cyanostilbene derivatives with aggregation induced emission properties, *J. Mol. Struct.*, 2025, **1322**, 140498.

44 L. Zhu and Y. Zhao, Cyanostilbene-based intelligent organic optoelectronic materials, *J. Mater. Chem. C*, 2013, **1**, 1059–1065.

45 B. Huang, Y. Ji, Z. Li, N. Zhou, W. Jiang, Y. Feng, B. Lin and Y. Sun, Simple aggregation–induced delayed fluorescence materials based on anthraquinone derivatives for highly efficient solution–processed red OLEDs, *J. Lumin.*, 2017, **187**, 414–420.

46 Z. Bai, X. Li, M. Wang, L. Xu, R. Jiang, B. Z. Tang and Z. Zhao, Efficient thermally activated delayed fluorescence materials from symmetric anthraquinone derivatives for high-performance red OLEDs, *Org. Electron.*, 2024, **135**, 107142.

47 B. Huang, W. C. Chen, Z. Li, J. Zhang, W. Zhao, Y. Feng, B. Z. Tang and C. S. Lee, Manipulation of molecular aggregation states to realize polymorphism, AIE, MCL, and TADF in a single molecule, *Angew. Chem.*, 2018, **130**, 12653–12657.

48 B. Huang, Z. Li, H. Yang, D. Hu, W. Wu, Y. Feng, Y. Sun, B. Lin and W. Jiang, Bicolour electroluminescence of 2-(carbazol-9-yl) anthraquinone based on a solution process, *J. Mater. Chem. C*, 2017, **5**, 12031–12034.

49 Y. Guo, Z. Wu, C. Wang, Y. Liang, F. Ji, Y. Wang, H. Zhang, X. Feng and G. Zhao, Elaborating the influence of substituent on energy gap and spin-orbit coupling of singlet-triplet excited states of novel organic light-emitting anthraquinone compounds in solution, *J. Lumin.*, 2021, **234**, 117964.

50 F. Hu, W. Yang, L. Li, J. Miao, S. Gong, C. Ye, X. Gao and C. Yang, Multifunctional emitters with TADF, AIE, polymorphism and high-contrast multicolor mechanochromism: Efficient organic light-emitting diodes, *Chem. Eng. J.*, 2023, **464**, 142678.

51 (*a*) A. Afrin and P. C. A. Swamy, Aggregation induced emission and reversible mechanofluorochromism active carbazole–anthracene conjugated cyanostilbenes with different terminal substitutions, *New J. Chem.*, 2023, **47**, 18919–18932; (*b*) A. Afrin, U. Adithyamol and P. C. A. Swamy, Donor Positional Inversion in Carbazole-Cyanostilbene Conjugates: Reorienting Connectivity for Solid-State Color Modulation, *Mater. Adv.*, 2025, DOI: 10.1039/D5MA00978B.

52 A. Afrin and P. C. A. Swamy, Tailoring Emission Color shifts in Mechanofluorochromic Active AIE Systems of Carbazole-Based D-π-A conjugates: Impact of π Spacer Unit Variants, *J. Org. Chem.*, 2024, **89**, 7946–7961.

53 A. Afrin and P. C. A. Swamy, π-Spacer Engineering: Driving Near-infrared Aggregation Induced-emission and Mechanofluorochromism in Carbazole-biscyanostilbenes, *Chem. – Eur. J.*, 2024, **31**, e202403644.

54 A. Afrin and P. C. A. Swamy, Structural modulations: unraveling the impact of benzothiazole positions on the optical properties of carbazole–cyanostilbenes, *CrystEngComm*, 2025, **27**, 3664.

55 A. M. Shaikh, S. Chacko and R. M. Kamble, Synthesis, optoelectronic and theoretical investigation of anthraquinone amine– based donor–acceptor derivatives, *ChemistrySelect*, 2017, **2**, 7620–7629.

56 A. Afrin and P. C. A. Swamy, Main-Group Synergy in Carbazole Emitters: Enhancing Cyanostilbene Solid-State Emission to Near Unity Quantum Yield *via* Duryl-Bridged Dimesitylborane, *Inorg. Chem.*, 2025, **64**, 17459–17469.

57 O. Anitha, M. Mathivanan, B. Tharmalingam, T. Thiruppathiraja, S. Ghorai, R. Natarajan, V. Thiagarajan, S. Lakshmipathi and B. Murugesapandian, Multi-stimuli responsiveness of pyrimidine bishydrazone: AIE, tuneable luminescence, white light emission, mechanochromism, acidochromism and its anticounterfeiting applications, *Dyes Pigm.*, 2023, **212**, 111091.

58 M. J. Frisch, G. W. Trucks, H. B. Schlegel, G. E. Scuseria, M. A. Robb, J. R. Cheeseman, G. Scalmani, V. Barone, G. A. Petersson, H. Nakatsuji, X. Li, M. Caricato, A. V. Marenich, J. Bloino, B. G. Janesko, R. Gomperts, B. Mennucci, H. P. Hratchian, J. V. Ortiz, A. F. Izmaylov, J. L. Sonnenberg, D. Williams-Young, F. Ding, F. Lipparini, F. Egidi, J. Goings, B. Peng, A. Petrone, T. Henderson, D. Ranasinghe, V. G. Zakrzewski, J. Gao, N. Rega, G. Zheng, W. Liang, M. Hada, M. Ehara, K. Toyota, R. Fukuda, J. Hasegawa, M. Ishida, T. Nakajima, Y. Honda, O. Kitao, H. Nakai, T. Vreven, K. Throssell, J. A. Montgomery Jr, J. E. Peralta, F. Ogliaro, M. J. overo Bearpark, J. J. Heyd, E. N. Brothers, K. N. Kudin, V. N. Star v, T. A. Keith, R. Kobayashi, J. Normand, K. Raghavachari, A. P. Rendell, J. C. Burant, S. S. Iyengar, J. Tomasi, M. Cossi, J. M. Millam, M. Klene, C. Adamo, R. Cammi, J. W. Ochterski, R. L. Martin, K. Morokuma, O. Farkas, J. B. Foresman and D. J. Fox, *Gaussian 09, Revision B.01*, Gaussian, Inc., Wallingford, CT, 2016.

59 C. Leyva-Porras, P. Cruz-Alcantar, V. Espinosa-Solís, E. Martínez-Guerra, C. I. Piñón-Balderrama, I. Compean Martínez and M. Z. Saavedra-Leos, Application of differential scanning calorimetry (DSC) and modulated differential scanning calorimetry (MDSC) in food and drug industries, *Polymers*, 2019, **12**, 5.